Available online at www.sciencedirect.com
ScienceDirect
Ceramics International 38 (2012) 679–685
CERAMICS INTERNATIONAL
www.elsevier.com/locate/ceramint

Colloidal stability–slip casting behavior relationship in slurry of mullite synthesized by the USP method

Remzi Gören [a], Bahri Ersoy [b], Cem Özgür [a,*], Talip Alp [c]

[a] Dumlupinar University, Department of Ceramic Engineering, Kütahya 43100, Turkey
[b] Afyonkocatepe University, Department of Materials Science and Engineering, Turkey
[c] University of Yalova, Faculty of Engineering, Turkey

Received 4 May 2011; received in revised form 21 July 2011; accepted 25 July 2011
Available online 30th July 2011

Abstract

This study presents the outcome of a research concerning the relationship between the colloidal stability of mullite powders synthesized by the USP (ultrasonic spray pyrolysis) method and its slip casting behavior. The colloidal stability of mullite slurry has been investigated under three different pH conditions (4.5, 8.9 and 10.9) derived from pH-dependent zeta potential (ZP) curves. Employing these pH values, mullite slurries with 50 wt.% solid content were prepared and slip cast. The microstructures of dried and sintered specimens were examined using SEM. It is concluded that the pH significantly influences the stability and in turn the slip casting behavior of the mullite slurry. In order to prepare homogeneous and stable mullite slurry for efficient slip casting it is preferable to utilize a basic rather than an acidic medium. High pH (i.e. 10.9) tends to leads to more closely packed mullite particles resulting in a homogeneous microstructure and greater structural integrity.

Keywords: A. Slip casting; D. Mullite; Zeta potential

1. Introduction

Mullite ($3Al_2O_3{\cdot}2SiO_2$) is becoming increasingly important in electronic, optical, and high temperature structural applications due to its attractive properties such as excellent high temperature strength, resistance to creep and thermal shock, low dielectric and thermal expansion constants [1]. Some important applications of mullite and/or mullite based ceramics include a matrix material for continuous fibre reinforced ceramic matrix composites (CMCs) used as thermal protection systems for combustion chambers in aircraft turbine engines and stationary gas turbines, heat exchange parts, heat insulating parts, milling media, furnace center tube, refractories in the metallurgical industries for electric furnace roofs, protective coatings, turbine engine components, hot metal mixers and low frequency induction furnaces [1–5].

Slip casting is an attractive and well established forming method for powder based shaping of ceramic components that has been used for a long time. It is widely used in the production of ceramics, due to its versatility as a consolidation process to obtain materials with high green density and microstructural homogeneity [6]. In this process, slurry containing a high proportion of solid with a high degree of stability is prerequisite for products with high green density. Unstable (or undispersed) slurry causes defects in the final sintered body which negatively affects the final mechanical and physical properties [7]. It is well known that there are two main operating repulsive forces which contribute to the stability of a colloidal suspension like ceramic slurry; (i) electrical double layer (EDL) and (ii) steric forces [7–10]. Steric repulsive forces between two particles generally occur when their surfaces are coated with a polymer based dispersant so that they prevent the particles from physical contact. However, the EDL forces between colloidal particles in a suspension occur when overlapping of the EDLs of two adjacent particles takes place and can be easily changed through changing of the suspension pH, or electrolyte/dispersant addition. Each mineral has an IEP (a certain pH value) controlled by the mineral powder's molecular constitution. In general, mineral powders typically flocculate (become unstable) at the IEP and they deflocculate (stabilize) as the pH increases or decreases away

* Corresponding author. Tel.: +90 274 265 20 31/4312; fax: +90 274 265 20 66.
E-mail address: cozgur@dumlupinar.edu.tr (C. Özgür).

0272-8842/$36.00 © 2011 Published by Elsevier Ltd and Techna Group S.r.l.
doi:10.1016/j.ceramint.2011.07.056

from IEP. Hence, if charge stabilization is the dominant stability mechanism for a suspension, then the zeta potential can be used to predict suspension stability [11].

The relevant literature cites several researches on the production and mechanical and physical properties of various mullite containing ceramic composites such as alumina/mullite, alumina/mullite/zirconia, mullite/zirconia, mullite/zirconia/zircon and cordierite/mullite formed by the slip casting method [12–20]. However, with the exception of the research carried out by Camerucci et al. (1998) no other study has been focused on suspension parameters such as pH, type and quantity of dispersant and their effects on the characteristics of green and sintered products. Camerucci et al. discussed the effect of solid content and dispersant (polyethylene glycol) on the viscosity of cordierite–mullite slurry, and consequently on the properties of both green and sintered products [20]. They have concluded that both parameters substantially influence the slip casting behavior of the slurry. Nevertheless, in order to fully determine the stability and flow characteristics, and explain the stabilization mechanisms of slurries containing different types of minerals, the stabilizing conditions for each constituent in the mixture must be identified. Published researches on the microstructural and physical properties of products manufactured from mullite alone by the slip casting are scanty [21–23]. Tkalcec et al. investigated the effect of sintering temperature on the mechanical properties and microstructure of products obtained by slip casting of refined mullite powders prepared by the sol–gel technique [22]. Burgos-Montes and Moreno, on the other hand, examined the effect of the dispersant on the stability of mullite slurry in which the mullite powders were produced by the ‘‘combustion synthesis’’ technique [23]. They obtained strong sintered products from mullite slurry with polyacrylic acid dispersant. The work of Hashi and Senna appears to be the only attempt to study the influence of pH on the stability of mullite slurry and in turn on the green and sintered products [21]. They examined the relationship between the pH and the rheology of mullite slurry and pore size distribution of the green compacts. They pointed out that product slip cast from shear thinning slurries prepared at pH 8 posses a larger total pore volume than those prepared with pH 4. The larger pore volume is attributed to the occurrence of agglomeration at pH 8 which is close to the pH 8.7 values corresponding to the IEP of mullite. The present research aims to contribute to the relevant literature by providing a detailed discussion on the effect of pH on the slip casting behavior of mullite slurry without dispersant, and consequently on the microstructure of green compacts and sintered products manufactured from mullite produced by the USP technique. Another objective of this investigation is to resolve the discrepancy between the IEP values of mullite reported by different researchers [21,23].

2. Materials and methods

2.1. Synthesizing and characterization of mullite powder

The USP system which was used for the preparation of mullite powders and the powder preparation steps involved are described in detail elsewhere [24]. The USP system consists of an ultrasonic nebulizer, a quartz tube and a powder collecting unit. The starting chemicals were tetraethylorthosilicate (TEOS, Fluka, of 98% purity) and aluminum nitrate nanohydrate ($Al(NO_3)_3{\cdot}9H_2O$, with extra pure Merck), containing silicon and aluminum species, respectively. For the preparation of the solution, TEOS with a molarity of 1.5 was added to distilled water and mixed with magnetic stirrer at 500 rpm to form a clear solution during which 0.2 M HNO_3 was added to the water. Finally, aluminum nitrate nanohydrate was dissolved with continued stirring to obtain the required solution. Clarity of solutions as measured by turbidimeter was regarded as acceptable when the turbidity value was below 0.1 NTU. The solution was placed in an ultrasonic nebulizer (frequency, 1.63 MHz) to produce aerosol in small droplets which were then conveyed through a quartz tube placed in a vertical furnace, where the constituents combine to form mullite. The air flow rate used was 1.5 l/min. The temperature of the tubular furnace was fixed at 1000 °C. The pyrolyzed powders were collected by filtration using membrane filters (Schleicher & Schuell-NL 16) having a pore size of 0.2 μm. The powders were then characterized by XRD (Rigaku™ miniflex), SEM (Leo-1430 VP) and FTIR (Bruker Vertex 70 series Fourier Transform Infrared Spectrometer) techniques. In addition, thermal decomposition of the solution was studied by TG/DTA (Perkin Elmer-Diamond) in ordinary air at a constant heating rate of 10 °C min^{-1}.

2.2. Zeta potential (ZP) and rheological measurements

In dilute aqueous solutions, the stability of the synthesized mullite powders was studied as a function of pH through ZP measurements that were performed using the electrophoresis method (ZetaSizer NanoZS model, Malvern, UK). The dilute suspensions were prepared by adding 0.4 g of the mullite powder into distilled water in a glass beaker. The ZP experiments were conducted for two different solutions which contained 10^{-3} M and 10^{-2} M NaCl respectively to maintain a constant ionic strength. 40 ml samples of the suspensions thus prepared were further stirred by magnetic mixer at 700 rpm for 2 min before and after pH adjustments. The solutions with varying pH values ranging from 2 to 12 were adjusted to the appropriate pH using stock solutions of KOH and H_2SO_4. pH measurements of solutions the were performed with a sensitivity of ±0.01. Prior to ZP measurements, ultrasonic vibrations were applied to prevent agglomeration and/or break up soft agglomerates at a 20 kHz frequency and 35% amplitude for 30 s.

The flow behavior of concentrated suspensions (slurries) of the mullite was determined using a rotational rheometer (Bohlin Instruments-CVO) with shear rate control. All rheological measurements were performed at the ambient temperature. Concentrated suspensions of powders were prepared to solid content of 50 wt.% without using a dispersing agent. The mullite slurries were prepared by adding 10.2 g of mullite powder to 10.2 g of aqueous solution, of 10^{-3} M NaCl. Homogenization was carried out by 6 h ball milling using alumina jar and balls. Prior to rheological measurements, pH adjustments of the

suspensions were performed at 4.65, 8.9 and 10.9, afterwards, they were stirred for 10 min. Flow curves plotted as shear stress versus shear rate, were obtained under controlled rate condition with a three-stage measuring program with a linear increase of the shear rate from 0.2 to 1000 s^{-1} for 2 min, a plateau at 1000 s^{-1} for 1 min, and a further decrease to 0.2 s^{-1} for 2 min.

2.3. Slip casting and microstructure analysis

The mullite slurries prepared at three different pH values (4.5, 8.9 and 10.9) were slip cast on plaster of Paris moulds to obtain solid discs (2 cm in diameter). After initially drying at room temperature for 48 h and subsequently at 105 °C for 24 h, the green cast products were sintered at 1600 °C using a heating rate of 5 °C min^{-1} and a soaking time of 5 h. SEM observations were performed on the gold-coated specimens after the drying and firing processes using the secondary electrons generated by SEM (Leo-1430 VP). In addition, percentage porosity of sintered specimens was measured by Hg-porosimetry (Quantachrome, Poremaster 60000).

3. Results and discussion

3.1. Characterization

The DTA/TG curves of the clear solution with the chemical constituents mentioned in Section 2.1 up to 1200 °C is presented in Fig. 1. In the DTA curve, there are three peaks at 125 °C, 250 °C and 990 °C two of which are endothermic and one is exothermic respectively. The endothermic peaks correspond to loss of H_2O, nitric acid, decomposition of TEOS and aluminum nitrate nanohydrate. The exothermic peak at around 990 °C indicates that the atomic scale solution prepared by mixing Al and Si species has converted directly to mullite [25–28]. Accordingly, it was thought that it may be possible to obtain mullite powders around 990 °C.

The mullite powders obtained by the USP method were characterized via XRD and FTIR techniques. X-ray analysis revealed the samples to be amorphous (Fig. 2). However,

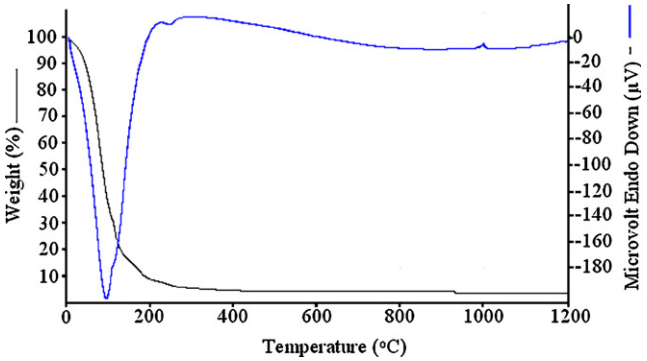

Fig. 1. DTA/TG curve of the solution.

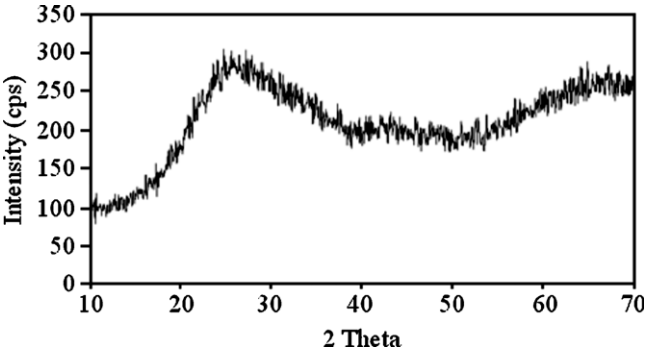

Fig. 2. XRD pattern of the mullite powder synthesized by the USP method at 1000 °C.

spectral analysis by FTIR (Fig. 3), a technique based on vibrations of the atoms of a molecule and successfully employed in the characterization of inorganic compounds (i.e. minerals) as well as organic compounds [29,30] revealed the sample to have mullite-like molecular groups. As in the case of silicate minerals, the two peaks appeared around at 3400 and 1600 cm^{-1} may be attributed to the OH stretching vibrations and the deformation vibration of adsorbed water, respectively [31]. The other peak located at 3750 cm^{-1} may be attributed to the OH stretching vibration arising from the Si–OH groups [32]. The shoulders around 1152 cm^{-1} and 456 cm^{-1} are

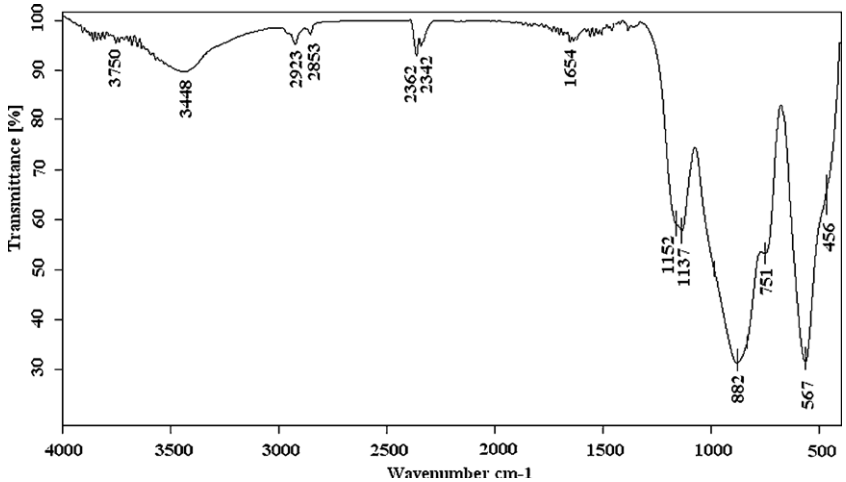

Fig. 3. FTIR spectrum of the mullite powder synthesized by the USP method at 1000 °C.

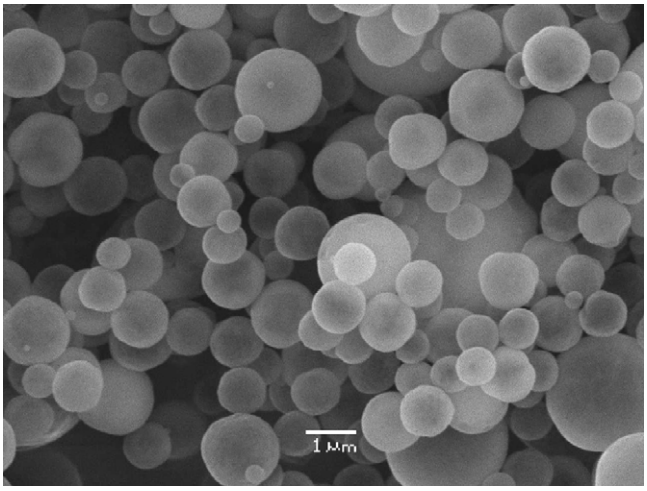

Fig. 4. SEM image of the mullite powder synthesized by the USP method at 1000 °C.

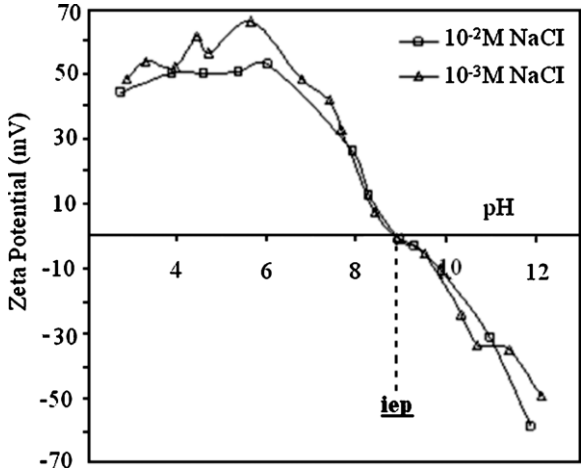

Fig. 5. Variation of zeta potential of mullite as a function of pH in the presence of indifferent electrolyte (NaCl).

assigned to vibrational mode of the asymmetric stretch of Si–O–Si and bending of Si–O–Si, respectively [33,34]. The band at 567 cm^{-1} is ascribed to Al–O stretching vibration modes resulting from AlO_6 groups of mullite [35,36]. The band at 751 cm^{-1} is in agreement with the proposed (Si,Al)–O–(Si,Al) bending mode for the band at 737 cm^{-1} in mullite [25]. According to the literature [37,38], the fundamental bands assigned to the SiO_4 (482, 988, 1107, 1131 and 1168 cm^{-1}), AlO_4 (620, 828 and 909 cm^{-1}), AlO_6 (578 and 482 cm^{-1}) and T–O–T (TO_4 where T means Si or Al) (737 cm^{-1}) show the presence and/or formation of the mullite. Both the literature and the bands at 567, 751, 882 and 1137 cm^{-1} appeared in the FTIR analysis indicate that the mullite powder produced by the USP technique includes amorphous mullite phase containing the short range order of AlO_6, SiO_4, AlO_4 and Si–O–Al linkages.

The SEM micrograph of the mullite powder obtained by USP at 1000 °C is shown in Fig. 4. The powder particles are shown to be of spherical shape with smooth surfaces and unagglomerated. The mean particle size is about 1.1 μm.

3.2. Determining the IEP (iso electric point) of mullite

The IEP of mullite was directly obtained by electrokinetic measurements of ZP against pH, in the presence of indifferent electrolytes of various molarities as seen in Fig. 5. The IEP also indicates that at this point (or pH) there is no charge at the surface, that is, the total positive charge is equal to the total negative charge. Electrokinetic studies revealed that the IEP for mullite was at pH 8.9. This is in agreement with the result of a study by Hashi and Senna [21]. Burgos-Montes and Moreno, on the other hand, have reported a pH value of 5.9 for the IEP of mullite produced by the combustion synthesis method in the presence of background electrolyte, 10^{-2} M of NH_4NO_3 [23]. However, according to the literature [9], in order to accurately determine the IEP of any mineral, its zeta potential measurements against pH must be performed in the presence of indifferent (or background) electrolytes which are usually monovalent symmetrical electrolytes such as chloride or nitrate salts of Na, K, NH_4 using two or three different molarities (i.e. 10^{-3}, 10^{-2}, 10^{-1} M). This is because the indifferent ions such as monovalent cations or anions are generally not able to adsorb in the IHP (Inner Helmholtz Plane) of the Stern layer in the electrical double layer (EDL) of a mineral particle. Hence, they cannot shift the IEP even when their concentration increases [39]. Consequently, as seen clearly in Fig. 5, the IEP of the mullite powders used in this study corresponds to a pH value of 8.9 which is very close to the IEP (pH 8.7) of crystalline mullite studied by Hashi and Senna [21]. However, there is a significant difference between the IEP values of mullite obtained from spray pyrolysis method used in the present study and the combustion synthesis method (pH 5.9) utilized by Burgos-Montes and Moreno [23]. As mentioned earlier, the FTIR spectrum of mullite obtained by the USP method (Fig. 3) shows that the sample has hydroxyl groups and/or water molecules bound to metallic atoms (Al or Si) in the structure. Unfortunately, no FTIR spectrum has been given for the mullite powder in the study due to Burgos-Montes and Moreno [23]. As is known from the literature [40] hydration increases the IEP, whereas dehydration decreases it. That is, as the thickness of the adsorbed water layer on the particle surface increases, the shear plane in the EDL can be expected to shift away from the surface thereby lowering the ZP, and in turn, shifting the IEP of the particle to lower pHs. Another plausible explanation for this divergence could be any contamination of the surface of mullite powders during production or pretreatments during ZP measurements. According to the relevant literature such a surface contamination may lead to vary the IEPs of mineral powders [41]. On the other hand, the zeta potential increases sharply with decrease in pH from zero mV at pH 8.9 to the about 50–60 mV at about pH 6 depending on the ionic strength of the medium due to dissociation of –MOH (where M symbolizes Si or Al) groups or proton (H^+) adsorption on these groups, e.g.

$$[-MOH + H^+ \rightarrow -MOH_2{}^+ \leftrightarrow -M^+ + H_2O]$$

Further decrease in pH does not affect ZP significantly. Beyond the IEP (pH 8.9), increase in pH reverses the surface charge of mullite from positive to the negative attaining the

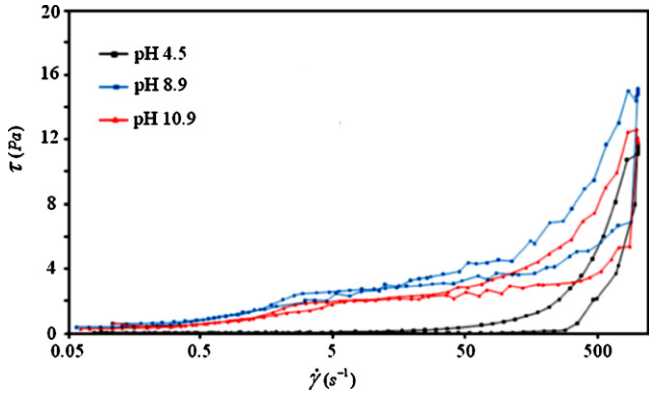

Fig. 6. Shear stress versus shear rate for mullite slurries prepared at different pHs.

level of −(30–33) mV at about pH 11 and ∼−60 mV at pH 12 due to the adsorption of OH– or deprotonation reactions, e.g.

$$[-\mathrm{MOH} + \mathrm{OH}^- \rightarrow -\mathrm{M(OH)_2}^- \leftrightarrow -\mathrm{MO}^- + \mathrm{H_2O}]$$

3.3. Shear stress versus shear rate curves

Stability of slurry with appropriate rheological properties coupled with high solid content and pseudoplastic (or shear-thinning) behavior is favored to yield products with high green density [21]. The flow curves obtained by plotting shear stress versus shear rate for mullite slip at pH 4.5, 8.9 (IEP) and 10.9 are presented in Fig. 6. All three slips displayed a pseudoplastic behavior. As shown in Fig. 6, the slurry exhibits a maximum shear stress at pH = 8.9 (IEP), a minimum at pH = 4.65 and intermediate at pH = 10.9. This is due to the fact that at IEP the EDL repulsive forces are non-existent so that particles cluster together under the influence of van der Walls forces of attraction. This in turn decreases the flow rate and increases the viscosity of the slurry. SEM data clearly support these findings (Fig. 7). Similarly, the ZP data is in a good agreement with the viscosity. The shear stress values of the mullite slurries obtained at the shear rates of 1000 s^{-1} and 10^{-3} M NaCl were 10.6, 14.8 and 12.3 Pa for pH 4.65, 8.9 and 10.9, respectively. Under the same pH conditions, the ZP values were +58, 0 and −33 mV, respectively. Similar results were obtained in a study undertaken by Hashi and Senna relating to the effect of pH on the zeta potential and viscosity of the mullite [21].

3.4. Microstructure analysis of green and sintered bodies

Green bodies were obtained by casting of the suspensions into a plaster mould. Fig. 7 depicts the fracture surfaces of dried green bodies as observed through the scanning electron microscope (SEM). The fracture surface of the specimens slip cast at pH 10.9, the SEM micrograph reveals 1–2 μm sized mullite particles with a relatively uniform size distribution. As clearly seen from Fig. 7b, mullite particles in the slurry cast at pH 8.9 (IEP) were totally agglomerated. That is, the packing of spherical mullite particles packed is irregular, inhomogeneous and loose. There seems to be no significant difference between the packing of the mullite particles in specimens cast from the slurries prepared under acidic (pH 4.5) and basic (pH 10.9) conditions respectively.

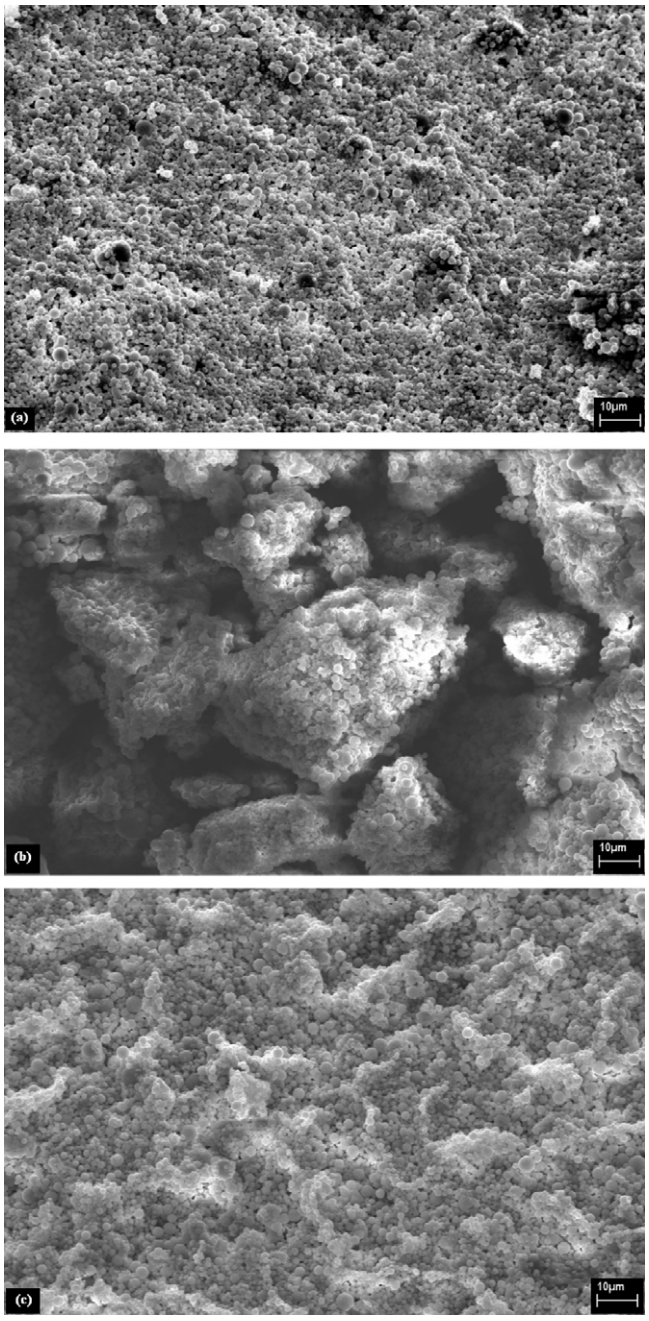

Fig. 7. SEM views of dried slip cast specimens prepared at (a) pH = 4.5, (b) pH = 8.9 (IEP) and (c) pH = 10.9.

Fig. 8 shows fracture surfaces of specimens slip cast and sintered at 1650 °C for 5 h. The SEM fractographs indicate that the spherical shaped mullite powders obtained by the USP tends to assume the well known rod-like structure after sintering at 1650 °C, while the mullite slip cast at pH 10.9 reveals an evidently more uniform size distribution and non-agglomerated surface. Indeed, when looked at Fig. 5 the absolute ZP of mullite powders at pH 10.9 (∼33 to 35 mV) is lower than that of pH 4.5 (∼48 to 53 mV) and thus it is expected that the packing of mullite powders at pH 4.5 is better than those at pH 10.9

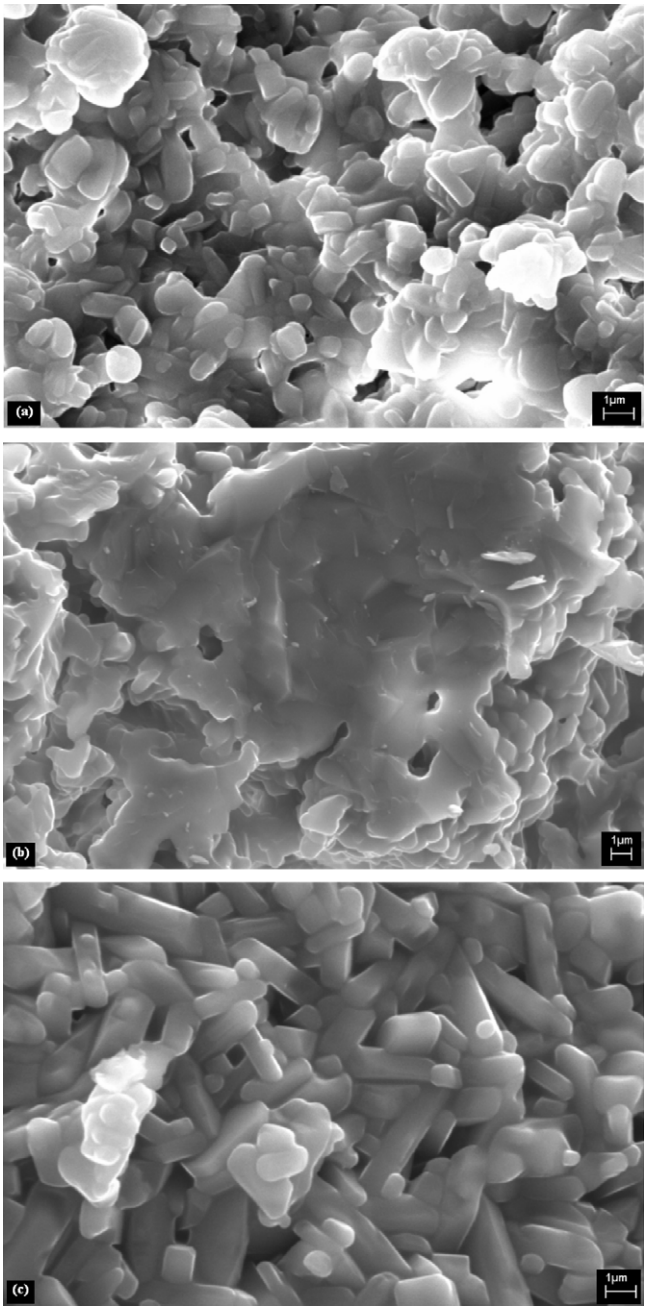

Fig. 8. SEM microstructures of slip cast specimens sintered at 1650 °C for 5 h: (a) pH = 4.5, (b) pH = 8.9 (IEP) and (c) pH = 10.9.

which will lead to more homogenous microstructure and a compact final product at pH 10.9. But for this contrariness, no explanation was found at present. It is important to note that comparison of Figs. 7b and 8b supports the notion that inhomogeneity and loose packing of particles in a green compact would lead to a non-homogeneous and loosely packed microstructure after sintering. Mercury-porosimetry measurements on sintered samples reinforce this view (Table 1). That is, the highest porosity (17.1 vol%) was obtained for the sintered sample slip cast at pH 8.9.

Table 1
Porosity (as vol%) values for the sintered samples slip cast at different pHs.

pH	% Porosity
4.5	8.2
8.9 (IEP)	17.1
10.9	7.5

4. Conclusions

- Using the ultrasonic spray pyrolysis (USP) method, it has been shown that the production of spherical mullite powders with average particle size of 1.1 μm and in narrow size range is feasible.
- The iso-electric point (IEP) for the mullite powders produced by the USP method has been determined as pH 8.9. As expected, at this pH the viscosity of the slurry is seen its maximum, while packing of mullite particles is the least closely packing.
- Mullite slurries prepared with 50% solid content and different pHs have been shown to exhibit pseudoplastic flow behavior.
- It has been possible to obtain mullite slurries of high stability by simply adjusting the pH level alone. However, SEM observations on cast and sintered products and also Hg-porosimetry measurements on sintered products have evidently shown that in order to increase the ZP of mullite as absolute value by pH adjustment, addition of basic electrolyte such as KOH rather than an acidic electrolyte yields better results.
- Notwithstanding the fact that the absolute ZP (∼33 to 35 mV) in the vicinity of pH 11 is lower than the absolute ZP (∼48 to 53 mV) obtained at pH 4.5, the microstructure of the product prepared from basic mullite slurry has been shown to be unequivocally more homogeneous. This condition leads to the development low porosity, in turn high density.

References

[1] I.A. Aksay, D.M. Dabbs, M. Sarikaya, Mullite for structural, electronic, and optical applications, J. Am. Ceram. Soc. 74 (10) (1991) 2343–2358.
[2] X.H. Jin, L. Gao, J.K. Guo, The structural change of diphasic mullite gel studied by XRD and IR spectrum analysis, J. Eur. Ceram. Soc. 22 (2002) 1307–1311.
[3] P. Mechnich, H. Schneider, M. Schmücker, B. Saruhan, Accelerated reaction bonding of mullite, J. Am. Ceram. Soc. 81 (7) (1998) 1931–1937.
[4] J.C. Chen, C.S. Chen, H. Schneider, C.C. Chou, W.C.J. Wei, Atomistic calculations of lattice constants of mullite with its compositions, J. Eur. Ceram. Soc. 28 (2008) 345–351.
[5] K. Yoshida, H. Hyuga, N. Kondo, H. Kita, Synthesis of precursor for fibrous mullite powder by alkoxide hydrolysis method, Mater. Sci. Eng. B 173 (2010) 66–71.
[6] Y. Takao, T. Hotta, K. Nakahira, M. Naito, N. Shinohara, M. Okumiya, K. Uematsu, Processing defects and their relevance to strength in alumina ceramics made by slip casting, J. Eur. Ceram. Soc. 20 (2000) 389–395.
[7] R. Greenwood, Review of the measurement of zeta potentials in concentrated aqueous suspensions using electroacoustics, Adv. Colloids Interface Sci. 106 (2003) 55–81.
[8] S.B. Johnson, G.V. Franks, P.J. Scales, D.V. Boger, T.W. Healy, Surface chemistry–rheology relationships in concentrated mineral suspensions, Int. J. Miner. Process. 58 (2000) 267–304.
[9] R.J. Hunter, Zeta Potential in Colloid Science, third printing, Academic Press Inc., San Diego, 1988.

[10] J.N. Israelachvili, Intermolecular and Surface Forces, second ed., Academic Press Inc., London, 1992.
[11] T.M. Riddick, Control of Colloid Stability Through Zeta Potential, Zeta-Meter Inc., New York, 1968, pp. 1–372.
[12] C. Aksel, The influence of zircon on the mechanical properties and thermal shock behaviour of slip-cast alumina–mullite refractories, Mater. Lett. 57 (2002) 992–997.
[13] C. Aksel, Mechanical properties and thermal shock behaviour of alumina–mullite–zirconia and alumina–mullite refractory materials by slip casting, Ceram. Int. 29 (2003) 311–316.
[14] C. Aksel, The effect of mullite on the mechanical properties and thermal shock behaviour of alumina–mullite refractory materials, Ceram. Int. 29 (2003) 183–188.
[15] F. Temoche, L.B. Garrido, E.F. Aglietti, Processing of mullite–zirconia grains for slip cast ceramics, Ceram. Int. 31 (2005) 917–922.
[16] L.B. Garrido, E.F. Aglietti, L. Martorello, M.A. Camerucci, A.L. Cavalieri, Hardness and fracture toughness of mullite–zirconia composites obtained by slip casting, Mater. Sci. Eng. A 419 (2006) 290–296.
[17] N.M. Rendtorff, L.B. Garrido, E.F. Aglietti, Effect of the addition of mullite–zirconia to the thermal shock behavior of zircon materials, Mater. Sci. Eng. A 498 (2008) 208–215.
[18] N. Rendtorff, L. Garrido, E. Aglietti, Mullite–zirconia–zircon composites: properties and thermal shock resistance, Ceram. Int. 35 (2009) 779–786.
[19] L.B. Garrido, E.F. Aglietti, Reaction-sintered mullite–zirconia composites by colloidal processing of alumina–zircon–CeO_2 mixtures, Mater. Sci. Eng. A 369 (2004) 250–257.
[20] M.A. Camerucci, A.L. Cavalieri, R. Moreno, Slip casting of cordierite and cordierite–mullite materials, J. Eur. Ceram. Soc. 18 (1998) 2149–2157.
[21] Y. Hashi, M. Senna, Relationship between rheological properties of slurries and pore size distribution of cast and compressed compacts of mullite, Powder Technol. 83 (June (3)) (1995) 187–191.
[22] E. Tkalcec, R. Nass, T. Krajewski, R. Rein, H. Schmidt, Microstructure and mechanical properties of slip cast sol–gel derived mullite ceramics, J. Eur. Ceram. Soc. 18 (August (8)) (1998) 1089–1099.
[23] O. Burgos-Montes, R. Moreno, Colloidal behaviour of mullite powders produced by combustion synthesis, J. Eur. Ceram. Soc. 27 (2007) 4751–4757.
[24] C. Özgür, O. Şan, Preparation of spherical and dense Na_2O–B_2O_3–SiO_2 glass powder by ultrasonic spray pyrolysis technique, J. Non-Cryst. Solids 356 (2010) 2794–2798.
[25] H. Tan, Y. Ding, J. Yang, Mullite fibres preparation by aqueous sol–gel process and activation energy of mullitization, J. Alloys Compd. 492 (2010) 396–401.
[26] D.R. Treadwell, D.M. Dabbs, I.A. Aksay, Mullite ($3Al_2O_3$–$2SiO_2$) synthesis with aluminosiloxanes, Chem. Mater. 8 (1996) 2056–2060.
[27] B. Bagchi, S. Das, A. Bhattacharya, R. Basu, P. Nandy, Nanocrystalline mullite synthesis at a low temperature: effect of copper ions, J. Am. Ceram. Soc. 92 (3) (2009) 748–751.
[28] F. He, W.T. Petuskey, Low temperature mullite crystallization in Al- and Si-alkoxide derived homogeneous gels, Mater. Lett. 63 (2009) 2631–2634.
[29] J.W. Salisbury, L.S. Walter, N. Vergo, D.M. D'Aria, Infrared (2.1–25 μm) Spectra of Minerals, The Johns Hopkins University Press, London, 1991
[30] B. Stuart, W.O. George, P. McIntyre, in: D.J. Ando (Ed.), Modern Infrared Spectroscopy, John Wiley & Sons Inc., New York, 1998, p. 175.
[31] A.L. Andrade, R.M. de, M. Turchetti-Maia, M.T.P. Lopes, C.E. Salas, R.Z. Domingues, In vitro bioactivity and cytotoxicity of chemically treated glass fibers, Mater. Res. 7 (2004) 635–638.
[32] R. Baranwal, M.P. Villar, R. Garcia, R.M. Laine, Flame spray pyrolysis of precursor as a route to nano-mullite powder: powder characterization and sintering behavior, J. Am. Ceram. Soc. 84 (2001) 951–961.
[33] A. Hamoudi, L. Khouchaf, C. Depecker, B. Revel, L. Montagne, P. Cordier, Microstructural evolution of amorphous silica following alkali–silica reaction, J. Non-Cryst. Solids 354 (2008) 5074–5078.
[34] Dj. Janackovic, V. Jokanovic, Lj. Kostic-Gvozdenovic, D. Uskokovic, Synthesis of mullite nanostructured spherical powder by ultrasonic spray pyrolysis, Nanostruct. Mater. 10 (1998) 341–348.
[35] B. Bagchi, S. Das, A. Bhattacharya, R. Basu, P. Nandy, Mullite phase enhancement in Indian kaolins by addition of vanadium pentoxide, Appl. Clay Sci. 47 (2010) 409–413.
[36] J. Temuujin, K. Okada, K.J.D. MacKenzie, Ts. Jadambaa, The Effect of water vapour atmosphere on the thermal transformation of kaolinite investigated by XRD, FTIR and solid state MAS NMR, J. Eur. Ceram. Soc. 19 (1998) 105–112.
[37] L.S. Cividanes, T.M.B. Campos, L.A. Rodrigues, D.D. Brunelli, G.P. Thim, Review of mullite synthesis routes by sol–gel method, J. Sol-Gel Sci. Technol. 55 (2010) 111–125.
[38] A. Beran, D. Voll, H. Schneider, Dehydration and structural development of mullite precursors: an FTIR spectroscopic study, J. Eur. Ceram. Soc. 21 (2001) 2479–2485.
[39] M.S. Çelik, B. Ersoy, Mineral nanoparticles: electrokinetics, in: J.A. Schwarz, C.I. Contescu, K. Putyera (Eds.), Encyclopedia of Nanoscience and Nanotechnology, Marcel-Dekker Inc., New York, 2004 pp. 1991–2005.
[40] G.A. Parks, The isoelectric points of solid oxides, solid hydroxides, and aqueous hydroxo complex systems, Chem. Rev. 65 (1965) 177–198.
[41] R.D. Kulkarni, P. Somasundaran, Effect of pretreatment on the electrokinetic properties of quartz, Int. J. Miner. Process. 4 (1977) 89–98.